

Stochastic background of gravitational waves emitted by magnetars

Stefania Marassi^{1*}, Riccardo Ciolfi^{1†}, Raffaella Schneider², Luigi Stella³, Valeria Ferrari¹

¹*Dipartimento di Fisica ‘G. Marconi’, Sapienza Università di Roma and Sezione INFN ROMA1, Piazzale Aldo Moro 5, 00185 Roma, Italy*

²*INAF/Osservatorio Astrofisico di Arcetri, Largo Enrico Fermi 5, 50125 Firenze, Italy*

³*INAF/Osservatorio Astronomico di Roma, Via di Frascati 33, 00040 Monteporzio Catone, Italy*

7 September 2010

ABSTRACT

Two classes of high energy sources in our galaxy are believed to host magnetars, neutron stars whose emission results from the dissipation of their magnetic field. The extremely high magnetic field of magnetars distorts their shape, and causes the emission of a conspicuous gravitational waves signal if rotation is fast and takes place around a different axis than the symmetry axis of the magnetic distortion. Based on a numerical model of the cosmic star formation history, we derive the cosmological background of gravitational waves produced by magnetars, when they are very young and fast spinning. We adopt different models for the configuration and strength of the internal magnetic field (which determines the distortion) as well as different values of the external dipole field strength (which governs the spin evolution of magnetars over a wide range of parameters). We find that the expected gravitational wave background differs considerably from one model to another. The strongest signals are generated for magnetars with very intense toroidal internal fields ($\sim 10^{16}$ G range) and external dipole fields of $\sim 10^{14}$, as envisaged in models aimed at explaining the properties of the Dec 2004 giant flare from SGR 1806-20. Such signals should be easily detectable with third generation ground based interferometers such as the Einstein Telescope.

Key words: gravitational waves - galaxies: formation -stars: Population II - cosmology: theory.

1 INTRODUCTION

It is well known that a variety of astrophysical processes are able to generate a stochastic gravitational wave background (GWB), with distinct spectral properties and features (Ferrari et al. 1999a; Ferrari et al 1999b; Schneider et al. 2000, 2001; Regimbau & Mandic 2008; Marassi et al. 2009). The detection of these astrophysical GWBs can provide insights into the cosmic star formation history and constrain some of the physical properties of compact objects, white dwarfs, neutron stars and black holes. Moreover, these signals may act as foreground noise for the detection of cosmological GWBs over much of the accessible frequency spectrum.

In this paper we consider the GWB produced by *magnetars*, i.e. neutron stars with extremely high magnetic fields. Two classes of sources of high energy radiation in our Galaxy, the soft gamma repeaters (SGRs) and anomalous X-ray pulsars (AXPs), are believed to host magnetars, that power their emission through the release of magnetic field energy. These two classes of high-energy sources share a number of features among which are the spin period in a fairly narrow and long range (in the 2 - 12 s range), the spin-down timescales ($10^4 - 10^5$ yr), the relatively faint persistent emission (typically $10^{34} - 10^{35}$ erg/s), the emission of sporadic short bursts ($\ll 1$ s) with peak luminosities in the $10^{36} - 10^{41}$ erg/s range (see e.g. Mereghetti 2008 and references therein).

To successfully account for the observed features of both SGRs and AXPs, the magnetar model envisages that the neutron star possesses an internal magnetic field with strength $B > 10^{15}$ G which comprises both a toroidal and a poloidal component. The external B-field, on the contrary, is expected to be poloidal; its dipole strength is usually inferred to be in the $10^{14} - 10^{15}$ G range, based on the observed spin-down rate (as well as other indications). Strong internal magnetic fields ($\sim 10^{15}$ to 10^{16} G) will induce significant quadrupolar deformations in the neutron star structure; these may generate a detectable gravitational wave signal,

* E-mail: stefania.marassi@roma1.infn.it

† E-mail: riccardo.ciolfi@roma1.infn.it

if their symmetry axis is not aligned with the spin axis (see e.g. Cutler (2002) and references therein).

Using population synthesis methods to evaluate the initial period and the magnetic field distributions of magnetars, Regimbau & de Freitas Pacheco (2006) computed the GWB due to a magnetar population, assuming a purely poloidal magnetic field configuration both inside of the star and in the magnetosphere. They found that the largest signal is obtained for a type I superconductor neutron star model, and that the resulting closure energy density peaks at $\Omega_{\text{GW}} \sim 10^{-9}$ around 1.2 kHz; this is well below the sensitivity of the first generation of detectors, but it might be an interesting target for future detectors, e.g. the Einstein Telescope¹, as discussed in detail in Regimbau & Mandic (2008).

In the present work, we reconsider the GWB generated by magnetars, by using the cosmic star formation rate density evolution predicted by the numerical simulation of Tornatore et al. (2007), and adopting several magnetar models recently proposed in the literature. As a first example, we use the purely poloidal configurations discussed in Regimbau & de Freitas Pacheco (2006). We then consider *twisted torus* configurations, recently discussed in Ciolfi et al. (2009, 2010) and in Ferrari (2010); in these models the poloidal component of the magnetic field extends throughout the star and in the magnetosphere, whereas the toroidal component is confined to a torus-shaped region inside the star. Finally, we consider the model in Stella et al. (2005) (see also Dall’Osso et al 2009), namely an internal field configuration dominated by the toroidal component with strength $\sim 2 \cdot 10^{16}$ G (core-averaged value), and a poloidal field of ordinary strength ($10^{14} - 10^{15}$ G). Our main purpose here is to assess how the uncertainties related to the internal magnetic field strength and its configuration affect the resulting GW signal and whether next-generation detectors will have the potential to reveal such a signal and shed light on the properties of magnetars.

The plan of the paper is as follows. In Section 2 we briefly describe the numerical simulation performed by Tornatore et al. (2007) that we use to predict the cosmic star formation rate evolution and the corresponding magnetar birthrate. In Section 3 we sketch out the main features of the single source spectrum which describe the gravitational emission of a single magnetar, and introduce the different magnetar models considered in this work. In Section 4, we present the resulting density parameter of the GWB, Ω_{GW} , and discuss its detectability. In Section 5 we discuss the effect of the wobble angle on the generated background and its relevance for the detection of the signal. Finally, in Section 6 we draw our conclusions.

Throughout our work we have adopted a Λ CDM cosmological model with parameters $\Omega_M = 0.26$, $\Omega_\Lambda = 0.74$, $h = 0.73$, $\Omega_b = 0.041$, in agreement with the three-year WMAP results (Spergel et al. 2007).

2 THE MAGNETARS BIRTH RATE EVOLUTION

Following Marassi et al. (2009), we use the cosmic star formation rate density evolution predicted by the numerical simulation of Tornatore et al. (2007). For the present study, we consider the formation rate of Population II stars only; for these we adopt a Salpeter Initial Mass Function (IMF) $\Phi(M) \propto M^{-(1+x)}$ with $x = 1.35$ (normalized between $0.1 - 100M_\odot$), in regions of the Universe which have been already polluted by the first metals and dust grains (Schneider et al. 2002, 2003; Omukai et al. 2005).

Regimbau & de Freitas Pacheco (2001) and Popov et al. (2009) derived the statistical properties of highly magnetized neutron stars ($B \geq 10^{14}$ G) by using population synthesis methods; they showed that neutron stars born as magnetars represent 8-10% of the total simulated population of neutron stars. Here we assume a fraction $f_{\text{MNS}} = 10\%$; we further assume that magnetar progenitors have masses in the $8M_\odot - 40M_\odot$ range. It should be noted that the mass range of magnetar progenitors is still debated (see for instance Ferrario & Wickramasinghe 2008; Davies et al. 2009). However, the range we consider is sufficiently large to include the proposed evolutionary models.

The top panel of Fig. 1 shows the redshift evolution of the cosmic star formation rate density inferred from the simulation².

The number of magnetars formed per unit time out to a given redshift z can be computed by integrating the cosmic star formation rate density, $\dot{\rho}_*(z)$, over the comoving volume element, while restricting the integral over the stellar IMF in the proper range of progenitor masses; that is

$$R_{\text{MNS}}(z) = f_{\text{MNS}} \int_0^z dz' \frac{dV}{dz'} \frac{\dot{\rho}_*(z')}{(1+z')} \int_{8M_\odot}^{40M_\odot} dM \Phi(M), \quad (1)$$

where the factor $(1+z)$ at the denominator accounts for the time-dilation effect, and the comoving volume element can be expressed as

$$dV = 4\pi r^2 \left(\frac{c}{H_0} \right) \epsilon(z) dz \quad (2)$$

$$\epsilon(z) = [\Omega_M(1+z)^3 + \Omega_\Lambda]^{-\frac{1}{2}}.$$

The result is shown in the bottom panel of Fig. 1.

3 MAGNETARS AS GRAVITATIONAL WAVE SOURCES

The gravitational wave energy spectrum emitted by a single source is

$$\frac{dE_{\text{GW}}}{df_e} = \dot{E}_{\text{GW}} \left| \frac{df_e}{dt} \right|^{-1}, \quad (3)$$

where f_e is the emission frequency. The gravitational wave luminosity of a neutron star with spin axis forming a wobble

² The results shown in Fig. 1 refer to the fiducial run in Tornatore et al. (2007) with a box of comoving size $L = 10h^{-1}$ Mpc and $N_p = 2 \times 256^3$ (dark+baryonic) particles.

¹ <http://www.et-gw.eu/>

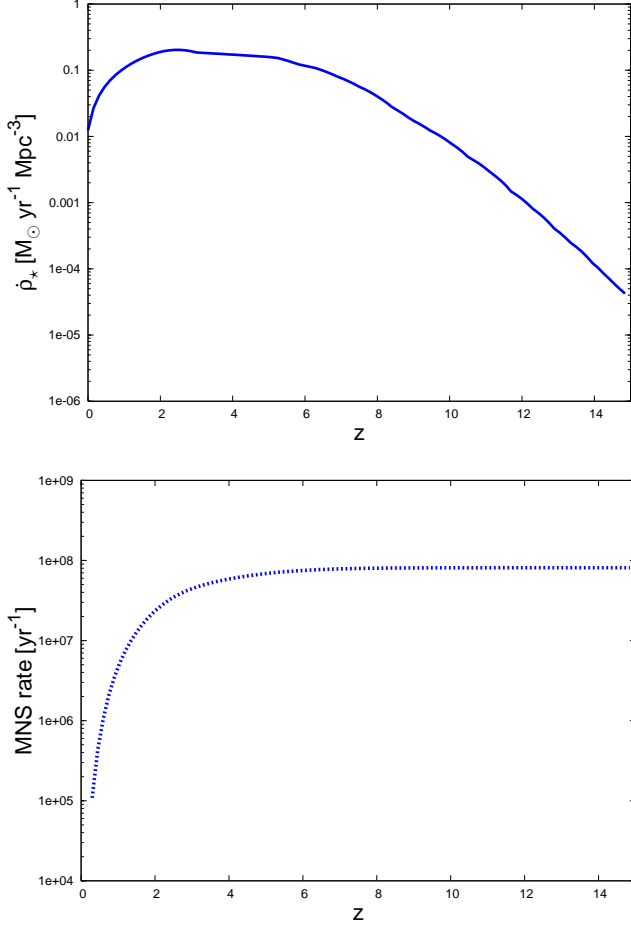


Figure 1. *Top panel:* redshift evolution of the comoving star formation rate density. *Bottom panel:* redshift evolution of the number of magnetars formed per unit time.

angle α with the magnetic axis is composed of two contributions, one at the spin frequency ν_R , one at its double $2\nu_R$; it can be written as

$$\dot{E}_{GW} = \frac{2G}{5c^5} I^2 \epsilon_B^2 \omega^6 \sin^2 \alpha (\cos^2 \alpha + 16 \sin^2 \alpha), \quad (4)$$

where ϵ_B is the star quadrupolar ellipticity induced by the magnetic field, ω is the angular velocity and I is the moment of inertia. The term $\sin^2 \alpha \cos^2 \alpha$ is from the emission component at the spin frequency, the term $16 \sin^4 \alpha$ from the component at twice the spin frequency.

In strongly magnetized neutron stars the quadrupolar deformation is determined essentially by the magnetic field configuration and strength³. Moreover, it depends on the equation of state of matter in the stellar interior.

The star loses rotational energy mainly due to electromagnetic radiation and gravitational wave emission (we shall neglect other effects, e.g. relativistic winds; Dall’Osso et al 2009). According to the well known vacuum dipole radiation model, the energy loss rate due to dipole radiation is given

³ Fast rotation will also induce a non-negligible deformation, which, being symmetric with respect to the spin axis, does not contribute to the gravitational wave emission.

by

$$|\dot{E}_{ROT}^{dip}| = \frac{1}{6} \frac{B_p^2 R^6}{c^3} \omega^4 \sin^2 \alpha, \quad (5)$$

where B_p is the field strength at the magnetic poles, and R the stellar radius. The total spin-down rate obtained from Eqs. (4) and (5) is

$$\begin{aligned} |\dot{\omega}| &= |\dot{\omega}^{dip}| + |\dot{\omega}^{GW}| \\ &= \frac{1}{6} \frac{B_p^2 R^6}{I c^3} \omega^3 \sin^2 \alpha + \frac{2G}{5c^5} I \epsilon_B^2 \omega^5 \sin^2 \alpha (1 + 15 \sin^2 \alpha). \end{aligned} \quad (6)$$

Using the above quantity and remembering that the first term of the gravitational wave luminosity given in Eq. (4) is emitted at $f_e = \nu_R = \omega/2\pi$, while the second at $f_e = 2\nu_R$, we can compute the single source emission spectrum according to Eq. (3).

The choice of the initial spin period P_0 for the neutron star population sets an upper limit on the frequency ranges where the two components of the GW emission contribute to the gravitational wave background: the emission at ν_R contributes to frequencies below $1/P_0$, that at $2\nu_R$ to frequencies below $2/P_0$. Therefore, for $f_e < 1/P_0$ the gravitational wave background has both contributions, while for $1/P_0 < f_e < 2/P_0$ the only contribution comes from the emission at $2\nu_R$. Hence, the terms to be considered when computing the spectral energy density of the background are:

for $f_e < \frac{1}{P_0}$,

$$\begin{aligned} \frac{dE_{GW}}{df_e} &= \frac{32\pi^4 G}{5c^5} I^2 \epsilon_B^2 f_e^3 \\ &\times \left\{ \cos^2 \alpha \left[\frac{B_p^2 R^6}{6Ic^3} + \frac{8\pi^2 G}{5c^5} I \epsilon_B^2 f_e^2 (1 + 15 \sin^2 \alpha) \right]^{-1} \right. \\ &\left. + \sin^2 \alpha \left[\frac{B_p^2 R^6}{6Ic^3} + \frac{2\pi^2 G}{5c^5} I \epsilon_B^2 f_e^2 (1 + 15 \sin^2 \alpha) \right]^{-1} \right\}; \quad (7) \end{aligned}$$

for $\frac{1}{P_0} < f_e < \frac{2}{P_0}$,

$$\begin{aligned} \frac{dE_{GW}}{df_e} &= \frac{32\pi^4 G}{5c^5} I^2 \epsilon_B^2 f_e^3 \\ &\times \sin^2 \alpha \left[\frac{B_p^2 R^6}{6Ic^3} + \frac{2\pi^2 G}{5c^5} I \epsilon_B^2 f_e^2 (1 + 15 \sin^2 \alpha) \right]^{-1}; \quad (8) \end{aligned}$$

for $f_e > \frac{2}{P_0}$,

$$\frac{dE_{GW}}{df_e} = 0.$$

If we assume $B_p = 10^{14} - 10^{15}$ G, $R \sim 10$ km, $I \sim 10^{45}$ g cm² and $f_e \lesssim 1$ kHz, we see that even for quadrupole ellipticities as large as 10^{-4} the term $\frac{B_p^2 R^6}{6Ic^3}$ is much larger than $\frac{8\pi^2 G}{5c^5} I \epsilon_B^2 f_e^2$; in this case the contribution of gravitational wave emission to the spin-down is negligible. As shown in the following, this holds in most of the cases we consider. It is worth noting that, when $\alpha \neq 0$ and $\frac{B_p^2 R^6}{6Ic^3} \gg \frac{8\pi^2 G}{5c^5} I \epsilon_B^2 f_e^2$, for $f_e < 1/P_0$ the dominant term in Eq. (7) is

$$\frac{dE_{GW}}{df_e} = \frac{32\pi^4 G}{5c^5} I^2 \epsilon_B^2 f_e^3 \left(\frac{B_p^2 R^6}{6Ic^3} \right)^{-1}, \quad (9)$$

which does not depend on the wobble angle α^4 . However, for $\frac{1}{P_0} < f_e < \frac{2}{P_0}$, the dominant term is

$$\frac{dE_{GW}}{df_e} = \frac{32\pi^4 G}{5c^5} I^2 \epsilon_B^2 f_e^3 \sin^2 \alpha \left(\frac{B_p^2 R^6}{6Ic^3} \right)^{-1}, \quad (10)$$

and it depends on α .

It should be stressed that in general the wobble angle depends on time. The misalignment of magnetic and rotation axes causes, in the neutron star frame, the free precession of the angular velocity around the magnetic axis with period $P_{prec} \simeq P/|\epsilon_B|$, where P is the spin period (Jones 2002; Jones & Andersson 2002). The star internal viscosity damps such precessional motion and reduces the wobble angle towards the aligned configuration ($\alpha = 0$), if the star has an oblate shape ($\epsilon_B > 0$), whereas it increases α towards the orthogonal configuration $\alpha = \pi/2$ (“spin-flip”), if the shape is prolate ($\epsilon_B < 0$) (Jones 1976; Cutler 2002). The second case is more favourable for gravitational wave emission.

The timescale of the process is given by $\tau_\alpha = nP_0/\epsilon_B$, where P_0/ϵ_B is the initial precession period and n is the expected number of precession cycles in which the process takes place; estimates for slowly rotating neutron stars indicate that $n \sim 10^2 - 10^4$ (Alpar & Sauls 1988), however the value of n is actually unknown (Cutler 2002). The evolution of the misalignment angle is relevant for our analysis only if the associated timescale, τ_α , is short compared to the spin-down timescale, τ_{sd} ; conversely, if $\tau_\alpha \gg \tau_{sd}$ the process takes place when the source is no longer an efficient gravitational wave emitter.

In principle, an accurate estimate of the GWB should account for (i) a proper distribution of the initial wobble angles for the magnetar population, and (ii) the evolution of such misalignment with time. This kind of analysis would, however, be affected by the wide uncertainties on both τ_α and the initial angle distribution. Nevertheless, as shown in Section 5, we found that, from the point of view of the GWB detectability, the value of α and its eventual change with time do not significantly affect the results. Since our main interest is focused on detection prospects, we proceed here with the simplifying assumption that all magnetars are born with $\alpha = \pi/2$ and that the misalignment evolution is ineffective. Then, in Section 5, we will consider the effects of a generic wobble angle.

An essential input for dE_{GW}/df_e is the magnetic field strength at the pole, B_p : it determines the electromagnetic spin-down rate and, depending on the model, it may also affect the stellar deformations. To be representative of the entire population, the value of B_p should be chosen as a suitable average. Such an average is uncertain at present; however the values of B_p inferred from AXPs and SGRs lie in the $10^{14} - 10^{15}$ G range (Mereghetti 2008). Our choice here is to span this range by studying its two extremes, $B_p = 10^{14}$ and 10^{15} G. As we shall see, this translates into an uncertainty in the results that is negligible in comparison with the uncertainties associated to our poor knowledge of the internal field configuration.

As we have seen, the overall GW emission depends on P_0 , the initial spin period. Following Regimbau & de Freitas Pacheco (2006) we set $P_0 = 0.8$ ms. For $\alpha = \pi/2$ this gives $f_e^{max} = 2/P_0 = 2500$ Hz. If $\alpha < \pi/2$, part of the gravitational wave emission is at the spin frequency and the corresponding contribution has a frequency cutoff $f_e^{max} = 1/P_0 = 1250$ Hz. The chosen value of P_0 implies a very fast spinning newborn neutron star, but still consistent with the believed range of neutron star spin rates at birth. We remark that, according to current scenarios of magnetar formation, strongly magnetized neutron stars are those that are born with periods of the order of ms, much faster than ordinary pulsars (Duncan & Thompson 1992). At the end of Section 4.1 we will sketch the effect of assuming lower initial spin frequencies.

In the following, we compute the gravitational wave background assuming different magnetic field models.

3.1 Purely poloidal magnetic field

The first two field configurations we consider describe a strongly magnetized neutron star endowed with a purely poloidal magnetic field, and have been used to evaluate the corresponding GWB in Regimbau & de Freitas Pacheco (2006).

It is well known that poloidal fields tend to make the star oblate ($\epsilon_B > 0$), while toroidal fields deform the star in a prolate shape ($\epsilon_B < 0$). Therefore, in the case we consider in this Section, ellipticity is always positive. Here we compute the gravitational wave emission according to Equations (7) and (8), setting, as in Regimbau & de Freitas Pacheco (2006), $\alpha = \pi/2$ and assuming that the viscous evolution of the wobble angle (which tends towards $\alpha = 0$ in the case of positive ellipticities, thus reducing GW emission) is slower than the spin-down of the star. For a given poloidal configuration of the internal B-field, the GW output is maximized under the above assumption.

The numerical inputs to compute dE_{GW}/df_e are B_p , ϵ_B , I and R . Following Konno et al. (2000), we write the quadrupolar ellipticity as

$$\epsilon_B = g \frac{B_p^2 R^4}{GM^2}, \quad (11)$$

where M is the mass of the star and the value of the dimensionless (deformation) parameter g accounts for the magnetic field geometry and the EOS. As in Regimbau & de Freitas Pacheco (2006), we consider two models with $g = 13$ (Model A) and $g = 520$ (Model B), respectively. The first model refers to an incompressible fluid star and a dipolar magnetic field (Ferraro 1954); similar values are obtained in relativistic models based on polytropic equations of state (Konno et al. 2000). Model B describes a scenario in which the neutron star core is a superconductor of type I, implying that the internal magnetic field is confined to the crustal layers (Bonazzola & Gourgoulhon 1996). This scenario gives much stronger deformations (see also Colaiuda et al. 2008).

As previously discussed, we adopt two different values of B_p : 10^{14} and 10^{15} G. The other parameters are fixed as follows: $R = 10$ km, $M = 1.4 M_\odot$ and $I = 10^{45}$ g cm².

⁴ It should be noted that if we remove the term $\sin^2 \alpha$ in Eq. (5) (see for instance Ostriker & Gunn 1969), the α dependence in Eq. (9) is preserved.

3.2 Twisted torus configurations

In order to account for the observed features of AXPs and SGRs, the magnetar model envisages that the internal magnetic field is a mixture of poloidal and toroidal components (Duncan & Thompson 1992; Thompson & Duncan 1993, 1995). A strong internal toroidal component is expected to form as a result of differential rotation shortly after the birth of neutron star. The magnetic energy stored in this component provides the energy reservoir to power the bulk of the magnetar emission throughout its lifetime, including short bursts and giant flares (Woods & Thompson 2006). The poloidal component of the B-field (or at least part of it) extends outside the star, giving rise to a magnetosphere. However, the detailed configuration of the magnetic field is presently unknown. Recent studies of the evolution of strongly magnetized stars in Newtonian gravity indicate that a particular magnetic field configuration, the so-called *twisted torus*, is a quite generic outcome of dynamical simulations and, due to magnetic helicity conservation, appears to be stable on dynamical time-scales (Braithwaite & Spruit 2004, 2006; Braithwaite & Nordlund 2006). In this model, the poloidal field extends throughout the star and the exterior, whereas the toroidal field is confined in a torus-shaped region inside the star.

Here we consider twisted torus equilibrium configurations of strongly magnetized neutron stars in the framework of general relativity (Ciolfi et al. 2009, 2010). The magnetic field includes contributions from higher multipoles ($l > 1$) coupled to the dipolar ($l = 1$) field which is usually assumed; an argument of minimal energy is adopted in order to establish the relative weights of the different multipoles as well as the relative strength of toroidal and poloidal fields. In this model the poloidal fields dominate over the toroidal ones. As a consequence, these stars have always an oblate shape (Ciolfi et al. 2009, 2010; Lander & Jones 2009). In order to account for the dependence on the equation of state, two different EOSs are employed, named APR2 and GNH3, which span a realistic range of compactness (Ciolfi et al. 2010).

As in the case of purely poloidal fields, we compute the gravitational wave emission spectrum according to Equations (7), (8) and assuming $\alpha = \pi/2$. For a given magnetic field strength ($B_p = 10^{14}$ and 10^{15} G) and stellar mass ($M = 1.4 M_\odot$), the model provides the ellipticity, radius and moment of inertia of the neutron star; we have

$$\epsilon_B \simeq k \left(\frac{B_p}{10^{15} \text{ G}} \right)^2 \cdot 10^{-6}, \quad (12)$$

with $k = 9$ (4), $R = 14.19$ (11.58) km, and $I = 1.82$ (1.33) $\cdot 10^{45}$ g cm², for the EOS GNH3 (APR2).

3.3 Toroidal-dominated magnetic field model

The last model we consider is based on the hypothesis of very strong toroidal fields inside the star. We assume a magnetic field configuration with an internal toroidal field of $\sim 2 \cdot 10^{16}$ G (core-averaged value), in addition to a poloidal field of ordinary strength ($10^{14} - 10^{15}$ G). Stella et al. (2005) showed that toroidal field strengths of this order are needed to explain the time-integrated emission of magnetars as inferred from the extremely bright giant flare that took place on 2004 December 27 from SGR 1806-20 (which liberated an energy

of 5×10^{46} erg). Giant flares of this magnitude could result from large-scale rearrangements of the core magnetic field or instabilities in the magnetosphere (Thompson & Duncan 2001; Lyutikov 2003). Such a huge toroidal field would induce prolate deformations as strong as $\epsilon_B \simeq -6.4 \cdot 10^{-4}$ (Cutler 2002). Consequently, a newly-born fast spinning magnetar is expected to emit a strong gravitational signal whose frequency, initially in the 0.5–2 kHz range, decreases over a timescale of days (and whose strain correspondingly decreases too). This signal should be observable with the Advanced Virgo/LIGO class detectors up the distance of the Virgo cluster (Dall’Osso et al 2009). The deformation associated to poloidal fields, whose strength is fixed by the choice of B_p , tends to oppose the above deformation; however in the cases considered here ($B_p = 10^{14}$ and 10^{15} G) the corresponding correction is negligible (of the order of $10^{-4} - 10^{-2}$, respectively). The physical inputs we use in Equations (7) and (8), in addition to $\alpha = \pi/2$, ϵ_B and B_p , are $R = 10$ km and $I = 10^{45}$ g cm².

The gravitational wave emission predicted by the present model with $B_p = 10^{14}$ G could be regarded as an upper limit among the different magnetar models (excluding exotic scenarios), as in this case there occurs the most favorable combination of magnetic fields: an extremely strong toroidal field dominates the deformation while the lower value of the poloidal field strength results in a slower spin-down. In addition, the shape of the star is prolate and the evolution of the wobble angle α leads the axis of the magnetically-induced deformation towards the orthogonal configuration, resulting in stronger gravitational wave emission.

3.4 Gravitational wave emission spectrum

We present here the gravitational wave spectrum emitted by the models illustrated above. In Fig. 2 we plot dE_{GW}/df_e as a function of the emitted frequency f_e for the two purely poloidal models A and B (hereafter P-A and P-B), the twisted torus model (hereafter TT) with the two equations of state considered (APR2, GNH3), and the toroidal-dominated model (hereafter TD). In the left (right) panel we assume $B_p = 10^{14}$ G ($B_p = 10^{15}$ G); as already discussed, these values define a likely range for B_p .

The first important indication which emerges from Fig. 2 is that the uncertainty related to the different magnetar models is always much higher (3-5 orders of magnitude) than the spread associated to the adopted range of B_p . Let us now focus on the $B_p = 10^{14}$ G case (left panel). The TD model is by far the most favorable for gravitational wave emission, having the optimal combination of strong deformation and slow electromagnetic spin-down. The second strongest emission is obtained with the P-B model, where large deformations are achieved even for this lower field strength. The emission predicted by the P-A model is lower by more than three orders of magnitude, due to the difference in the g^2 factor appearing in the expression of dE_{GW}/df_e . The two TT models are expected to give even weaker signals; they differ for the assumed EOS and, as expected, the one which gives less (more) compact stars, GNH3 (APR2), is associated to stronger (weaker) deformations and gravitational wave emission.

If we consider higher external poloidal fields ($B_p = 10^{15}$

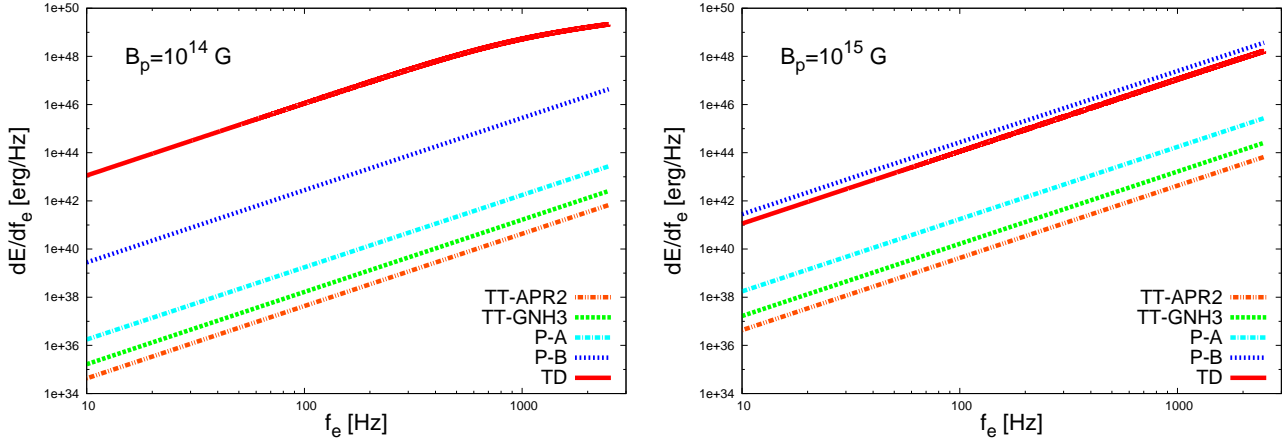


Figure 2. Spectral gravitational energy emitted by a single source as a function of the emitted frequency, for the different models we consider: P-A and P-B stand for the purely poloidal models A and B, TT are the twisted torus model predictions for the two EOS considered (APR2 and GNH3), TD indicates the toroidal-dominated model. *Left panel:* $B_p = 10^{14}$ G; *right panel:* $B_p = 10^{15}$ G.

G, right panel) the picture changes. For the P-A, P-B and TT models the value of B_p controls both the gravitational wave luminosity, which scales as B_p^4 ($\epsilon_B \propto B_p^2$), and the spin-down rate, which has the electromagnetic contribution proportional to B_p^2 plus a very small correction due to gravitational wave emission. As a result, $dE_{GW}/df_e \propto B_p^2$, which translates in a factor 100 increase from $B_p = 10^{14}$ to 10^{15} G. Conversely, in the TD model the deformation is determined by the dominant toroidal field in the stellar interior (with poloidal field corrections up to $\sim 1\%$ for 10^{15} G), and an increase in B_p only results in a higher electromagnetic spin-down and in a smaller overall gravitational wave emission. As long as the electromagnetic spin-down dominates over the gravitational wave spin-down, dE_{GW}/df_e is reduced by a factor of 100 from $B_p = 10^{14}$ to 10^{15} G. The final result is that when $B_p = 10^{15}$ G, the prediction of TD and P-B models are comparable.

It is worth noting that in all the considered models the contribution given by the gravitational wave emission to the spin-down is negligible, with the exception of the early time evolution in the TD model with $B_p = 10^{14}$ G (hereafter TD₁₄). This is shown in Fig. 2, where the energy spectra are linear in logarithmic scale, reflecting the behaviour $dE_{GW}/df_e \propto f_e^3$, while the TD₁₄ model is characterized by a lower emission level at high frequency, due to a non-negligible gravitational wave spin-down. This effect is even more evident in Fig. 3, where we compare the gravitational wave spectrum for the same TD model shown in the left panel of Fig. 2 with a TD model where gravitational wave spin-down is neglected (dashed line). It is clear that the gravitational wave contribution starts to be relevant at $f_e \sim 300$ Hz. For all the other models we have discussed, this contribution becomes relevant at much higher emission frequencies.

4 GRAVITATIONAL WAVE BACKGROUND FROM MAGNETARS

In this Section we compute the GWBs produced by the different magnetar models presented in the previous Section.

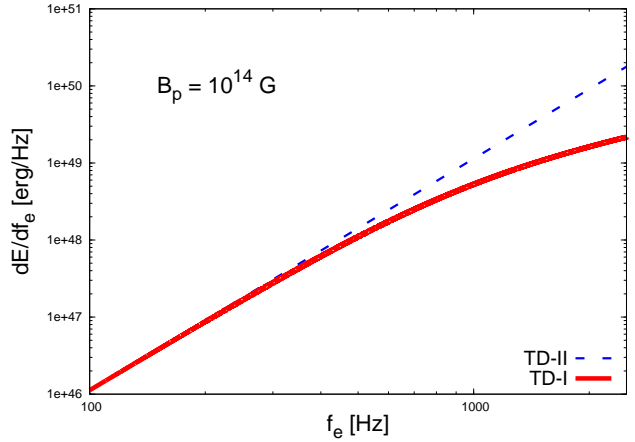


Figure 3. Spectral gravitational energy emitted by a single source according to the toroidal-dominated model as a function of the emitted frequency. TD-I is the same as TD in the left panel of Fig. 2; in TD-II (dashed line) the contribution of gravitational wave emission to the spin-down is neglected.

Following Marassi et al. (2009), the spectral energy density of the GWB can be written as

$$\frac{dE}{dSdfdt} = \int_0^{z_f} \int_{M_i}^{M_f} dR(M, z) \left\langle \frac{dE}{dSdf} \right\rangle, \quad (13)$$

where $dR(M, z)$ is the differential source formation rate

$$dR(M, z) = \frac{\dot{\rho}_*(z)}{(1+z)} \frac{dV}{dz} \Phi(M) dM dz, \quad (14)$$

and $\left\langle \frac{dE}{dSdf} \right\rangle$ is the locally measured average energy flux emitted by a source at distance r . For sources at redshift z it becomes

$$\left\langle \frac{dE}{dSdf} \right\rangle = \frac{(1+z)^2}{4\pi d_L(z)^2} \frac{dE_{GW}}{df_e} [f(1+z)], \quad (15)$$

where $f = f_e(1+z)^{-1}$ is the redshifted emission frequency f_e , and $d_L(z)$ is the luminosity distance to the source.

It is customary to describe the GWB by a dimensionless quantity, the closure energy density $\Omega_{GW}(f) \equiv$

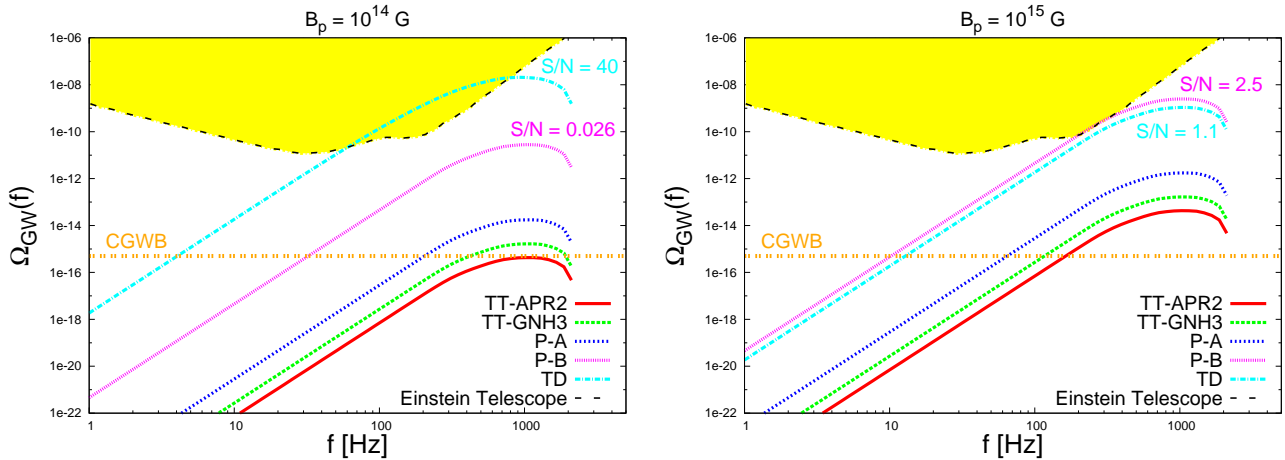


Figure 4. The predicted closure energy density (Ω_{GW}) as a function of the observational frequency, for the different magnetar models discussed in this paper: P-A and P-B stand for purely poloidal models A and B, TT are the twisted torus model predictions for the two EOS considered (APR2 and GNH3), TD is the toroidal-dominated model. *Left panel:* $B_p = 10^{14}$ G; *right panel:* $B_p = 10^{15}$ G. In both panels the shaded region indicates the foreseen sensitivity of the Einstein Telescope, and the horizontal dotted line (CGWB) is the upper limit on primordial backgrounds generated during the Inflationary epoch. A given background is detectable by the Einstein Telescope if the corresponding signal-to-noise ratio is larger than the detection threshold $S/N = 2.56$ (see text).

$\rho_{cr}^{-1}(d\rho_{gw}/d\log f)$, which is related to the spectral energy density by the equation

$$\Omega_{\text{GW}}(f) = \frac{f}{c^3 \rho_{cr}} \left[\frac{dE}{dS df dt} \right], \quad (16)$$

where $\rho_{cr} = 3H_0^2/8\pi G$ is the cosmic critical density.

In Fig. 4, we show Ω_{GW} as a function of the observational frequency for the different magnetar models. Differences in the predicted stochastic backgrounds reflect differences in the corresponding single magnetar emission spectrum. The maximum amplitude is always achieved around 1 kHz: in the left panel, it ranges from $\sim 4 \cdot 10^{-16}$ to $\sim 2 \cdot 10^{-8}$, while in the right panel the range is $\sim 4 \cdot 10^{-14}$ – $2 \cdot 10^{-9}$. The higher value is obtained with the TD model in the first case, and with the P-B model in the second case; the lower value is given in both cases by the TT-APR2 model. In both panels, model predictions are compared with the foreseen sensitivity of the Einstein Telescope (shaded region) and with the upper limit to primordial backgrounds generated during the Inflationary epoch (horizontal dotted line labelled CGWB). The latter contribution is estimated from Eq. (6) of Turner (1997) assuming a tensor/scalar ratio of $r = 0.3$ and no running spectral index of tensor perturbations (Kinney et al. 2006, 2008).

It is clear from the figure that the background generated by magnetars in the kHz region is higher than the primordial background, independently of the specific magnetar model considered; in addition, specific magnetar models lead to a cumulative signal which is potentially detectable by the Einstein Telescope. A more quantitative assessment of the detectability is reported in the following Section.

4.1 Detectability

The gravitational wave signal produced by the magnetar population can be treated as continuous. Indeed, if $\Delta\tau_{\text{gw}}$ is the average time duration of a signal produced by a single magnetar, and $dR(z)$ is the number of sources formed per

unit time at redshift z , the duty cycle D out to redshift z , defined as

$$D(z) = \int_0^z dR(z) \Delta\tau_{\text{gw}} (1+z), \quad (17)$$

satisfies the condition⁵ $D \gg 1$. Consequently, the stochastic signal appears in the detector outputs as a time-series noise which, by the central limit theorem, is expected to have a Gaussian-normal distribution function. In this case, as suggested by Allen & Romano (1999); Regimbau & Mandic (2008), the optimal detection strategy is to cross-correlate the output of two (or more) detectors, assumed to have independent spectral noises.

The optimized S/N for an integration time T is given by Allen & Romano (1999),

$$\left(\frac{S}{N} \right)^2 = \frac{9H_0^4}{50\pi^4} T \int_0^\infty df \frac{\gamma^2(f) \Omega_{\text{GW}}^2(f)}{f^6 P_1(f) P_2(f)}, \quad (18)$$

where $P_1(f)$ and $P_2(f)$ are the power spectral noise densities of the two detectors, and γ is the normalized overlap reduction function, characterizing the loss of sensitivity due to the separation and the relative orientation of the detectors.

The sensitivity of detector pairs is given in terms of the minimum detectable amplitude for a flat spectrum Ω_{MIN} ($\Omega_{\text{MIN}} = \text{const}$) defined as

$$\Omega_{\text{MIN}} = \frac{1}{\sqrt{T}} \frac{10\pi^2}{3H_0^2} \left[\int_0^\infty df \frac{\gamma^2(f)}{f^6 P_1(f) P_2(f)} \right]^{-1/2} \cdot (\text{erfc}^{-1}(2\alpha) - \text{erfc}^{-1}(2\gamma)), \quad (19)$$

where T is the observation time, α the false alarm rate, γ the detection rate and erfc^{-1} the complementary error function (for more details see Allen & Romano 1999).

If we consider the cross-correlation of two detectors with

⁵ If we take $\Delta\tau_{\text{gw}} = \tau_{sd}$ we have always D higher than 10^3 .

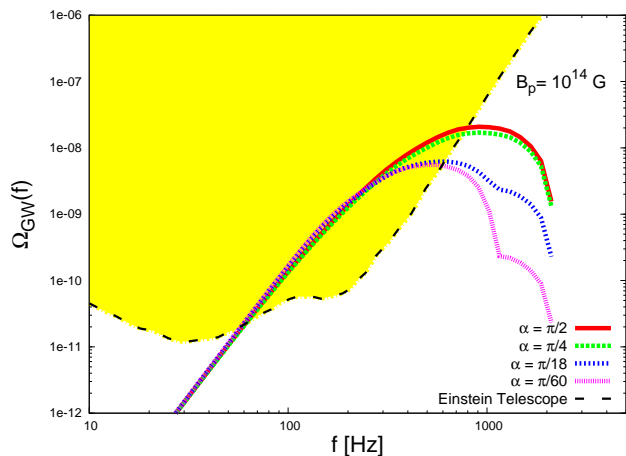


Figure 5. The TD_{14} background is plotted for different wobble angles, spanning the range $\pi/60 - \pi/2$, and compared with the Einstein Telescope sensitivity.

the sensitivity of the Einstein Telescope (T. Regimbau, private communication), we get $\Omega_{\text{MIN}} = 1.13 \cdot 10^{-11}$ for an integration time T of one year, a false alarm rate $\alpha = 10\%$ and a detection rate $\gamma = 90\%$; these values, inserted in Eq. (18), lead to a detection threshold S/N of 2.56.

A given background is detectable by the Einstein Telescope if the corresponding signal-to-noise ratio given by Eq. (18) is larger than the detection threshold. For instance, the predicted Ω_{GW} for the purely poloidal model P-B with $B_p = 10^{15}$ G gives $S/N = 2.49$, that is slightly smaller than such threshold; consequently, there is no chance to detect this signal. Conversely, in the most optimistic magnetar model TD_{14} (toroidal-dominated model with $B_p = 10^{14}$ G) we obtain $S/N = 40$, a very promising value. This result leads to the conclusion that third-generation gravitational wave detectors, such as the Einstein Telescope, hold the potential to reveal the cumulative GW signal from magnetars in the universe.

It is worth noting that the above results refer to the assumed initial spin period of $P_0 = 0.8$ ms. A higher value would lead to a lower frequency cutoff and, consequently, to a weaker GWB. For the TD_{14} model, for example, the detection threshold $S/N = 2.56$ corresponds to $P_0 = 5.2$ ms. Hence the GWB would still be detectable up to this value.

5 WOBBLE ANGLE EFFECTS

So far we have assumed a constant misalignment $\alpha = \pi/2$ between the spin and the magnetic axis, in which case the GW signal is emitted only at twice the spin frequency $f_e = 2\nu_R = \omega/\pi$. For a generic misalignment, we have also the emission at the spin frequency.

We now focus on the model TD_{14} and explore the consequences of $\alpha < \pi/2$. In this model the stellar deformation induced by the magnetic field are larger; being the most optimistic model for gravitational wave emission, this case allows to clearly show the effects of the wobble angle on detectability.

In Fig. 5 we compare the sensitivity of the Einstein Telescope with the background generated by model TD_{14}

for different (constant) values of the wobble angle. The plot clearly shows that when $\alpha \gtrsim \pi/4$ there is a single dominant contribution with the frequency cutoff at 2500 Hz, while for smaller angles there is a dominant contribution with $f^{\text{max}} = 1250$ Hz and a secondary contribution with lower amplitude extending up to $f^{\text{max}} = 2500$ Hz. Similar effects hold for the alternative magnetar models which have been presented in the previous Sections. A difference between the models potentially arises if the timescale for the evolution of the wobble angle is short compared to the spin-down timescale (see Section 3): in this case, the star rapidly tends (i) to the orthogonal configuration for the TD model, thus increasing gravitational wave emission, and (ii) to the aligned configuration, for models P-A, P-B and TT models, thus decreasing the emission.

As shown in Fig. 5, for the TD_{14} model (as well as for the other models) the gravitational wave backgrounds corresponding to different wobble angles exhibit significant differences at large frequencies, approximately above ~ 800 Hz, where the Einstein Telescope sensitivity is too low even for this model; therefore, the signal detectability is only marginally affected. Variations in the signal-to-noise ratio are at most 2-3% in the TD_{14} case, and if the gravitational wave background is weaker (e.g. for $B_p > 10^{14}$ G) the effects on the S/N are even smaller.

We can conclude that the initial value of α and its evolution in time do not have significant effects on the GWB detectability with the Einstein Telescope.

6 CONCLUSIONS

In this paper, we estimated the GWB produced by magnetars. We used a cosmic star formation history obtained from a numerical simulation performed by Tornatore et al. (2007) and assume that 10% of stellar progenitors with masses in the range $8 - 40M_\odot$ lead to magnetars with magnetic field strength in the $10^{14} - 10^{15}$ G range.

Since our present understanding of the physical properties of magnetars is still poor (the internal structure of the magnetic field and initial spin frequency being among the major uncertainties), we have explored the consequences for gravitational wave emission of different magnetar models proposed in the literature.

Our analysis shows that different models produce a spread in the resulting gravitational wave emission which is much higher than that produced by adopting different values for the magnetic field strength. In particular, we find that:

- Toroidal-dominated models, with an internal toroidal field of $\sim 2 \cdot 10^{16}$ G and an external poloidal field of 10^{14} G, proposed by Stella et al. (2005) to explain the 2004 giant flare from SGR 1806-20, generate the largest gravitational wave background, which could be detected in the frequency range between ~ 50 and ~ 600 Hz by third generation gravitational wave detectors such as the Einstein Telescope. Using correlated analysis of Einstein Telescope outputs, the estimated signal-to-noise ratios could be as high as 40.
- When larger poloidal fields, 10^{15} G, are considered, the largest gravitational background is generated by magnetar models with purely poloidal fields, and a superconductor

type-I core; in this case, the internal magnetic field is confined to the crustal layers, leading to strong deformations. Since deformations are produced by the internal toroidal field, Toroidal-dominated models are less effective because the increase in the poloidal field strength leads to a higher electromagnetic spin-down and to a lower gravitational wave emission.

- A comparison between the estimated magnetar GWB and the upper limit to the primordial background predicted by Inflationary scenarios (the horizontal dotted line in Fig. 4 labelled CGWB) shows that, for the models of magnetar we consider, the magnetar GWB is always larger than the primordial background in some region of frequency (the only exception is the twisted-torus model TT-APR2 with $B_p = 10^{15}$ G). For instance, for the toroidal dominated models TD₁₅ and TD₁₄ this is true, respectively, for $f \gtrsim 13$ Hz and $f \gtrsim 4$ Hz. Thus, the GWB generated by magnetars may act as a limiting foreground for the future detection of the primordial background even at frequencies as low as few tens of Hz.

We have also investigated the consequences on the resulting gravitational wave background of different values for the misalignment angle between the rotation and magnetic field axes. We find the largest effects to be at high frequencies, above ~ 800 Hz; thus the detectability of the largest backgrounds with the Einstein Telescope is only marginally affected, with fractional variations of the signal-to-noise ratios of at most 2-3%.

ACKNOWLEDGMENTS

We thank Tania Regimbau for useful suggestions and discussions and for providing us the ET correlated sensitivity curve and γ function.

Stefania Marassi thanks the Italian Space Agency (ASI) for the support. This work is funded with the ASI CONTRACT I/016/07/0.

This work was also supported by CompStar, a Research Networking Programme of the European Science Foundation.

REFERENCES

- Allen B., Romano J. D., 1999, *Phys. Rev. D* 59, 102001
 Alpar M. A., Sauls J. A., 1988, *ApJ* 327, 723
 Bonazzola S., Gourgoulhon E., 1996, *A&A* 312, 675
 Braithwaite J., Spruit H. C., 2004, *Nature* 431, 819
 Braithwaite J., Nordlund Å., 2006, *A&A* 450, 1077
 Braithwaite J., Spruit H. C., 2006, *A&A* 450, 1097
 Ciolfi R., Ferrari V., Gualtieri L., Pons J. A., 2009, *MNRAS* 397, 913
 Ciolfi R., Ferrari V., Gualtieri L., 2010, *MNRAS* 406, 2540
 Colaiuda A., Ferrari V., Gualtieri L., Pons J. A., 2008, *MNRAS* 385, 2080
 Cutler C., 2002, *Phys. Rev. D.* 66, 084025
 Cutler C., Jones D. I., 2001, *Phys. Rev. D.* 63, 024002
 Dall’Osso, S., Shore, S. N., & Stella, L., 2009, *MNRAS* 398, 1869
 Davies B., Figer D. F., Kudritzki R. P., Trombly C., Kouveliotou C., Wachter S., 2009, *ApJ*, 707, 844
 Duncan R. C., Thompson C., 1992, *ApJ* 392, L9
 Ferrari V., Matarrese S., Schneider R., 1999, *MNRAS* 303, 247
 Ferrari V., Matarrese S., Schneider R., 1999, *MNRAS* 303, 258
 Ferrari V., 2010, *CQG* to appear
 Ferrario L., Wickramasinghe D., 2008, *MNRAS* 389, L66
 Ferraro V. C. A., 1954, *ApJ* 119, 407
 Kinney W. H., Kolb E. W., Melchiorri A., Riotto A., 2006, *Phys. Rev. D.* 74, 023502
 Kinney W. H., Kolb E. W., Melchiorri A., Riotto A., 2008, *Phys. Rev. D.* 78, 087302
 Konno K., Obata T., Kojima Y., 2000, *A&A* 356, 234
 Jones P. B., 1976, *Ap&SS* 45, 669
 Jones D. I., 2002, *CQG* 19, 1255
 Jones D. I., Andersson N., 2002, *MNRAS* 331, 203
 Lander S. K., Jones D. I., 2009, *MNRAS* 395, 2162
 Lyutikov M., 2003, *MNRAS* 346, 540
 Marassi S., Schneider R., Ferrari V., 2009, *MNRAS* 398, 293
 Mereghetti S., 2008, *As. Ap. Rev.* 15, 225
 Omukai K., Tsuribe T., Schneider R., Ferrara A., 2005, *ApJ* 626, 627
 Ostriker J.P., Gunn J.E., 1969, *ApJ* 157, 1395
 Regimbau T., de Freitas Pacheco J. A., 2001, *A&A* 374, 182
 Regimbau T., de Freitas Pacheco J. A., 2006, *A&A* 447, 4
 Regimbau T., Mandic V., 2008, *CQG* 25, 184018
 Popov S. B., Pons J. A., Miralles J. A., Boldin. P. A., Posselt B., 2009, *MNRAS* 401, 2675
 Schneider R., Ferrara A., Ciardi B., Ferrari V., Matarrese S., 2000, *MNRAS* 317, 385
 Schneider R., Ferrari V., Matarrese S., Portegies-Zwart S., 2001, *MNRAS* 324, 797
 Schneider R., Ferrara A., Natarajan P., Omukai K., 2002, *ApJ* 571, 30
 Schneider R., Ferrara A., Salvaterra R., Omukai K., Bromm V., 2003, *Nature* 422, 869
 Stella L., Dall’Osso S., Israel G. L., Vecchio A., 2005, *ApJ* 634, L165
 Spergel D. N. et al., 2007, *ApJS* 170, 377
 Thompson C., Duncan R. C., 1993, *ApJ* 408, 194
 Thompson C., Duncan R. C., 1995, *MNRAS* 275, 255
 Thompson C., Duncan R. C., 2001, *ApJ* 561, 980
 Tornatore L., Ferrara A., Schneider R., 2007, *MNRAS* 382, 945
 Turner M.S., 1997, *Phys. Rev. D.* 55, R435
 Woods P. M., Thompson C., 2006, in "Compact Stellar Sources", ed. W. H. G. Lewin & M. van der Klis, (Cambridge: Cambridge Univ. Press) p. 547586